Journal of Power Sources 261 (2014) 156–161

Contents lists available at ScienceDirect

Journal of Power Sources

journal homepage: www.elsevier.com/locate/jpowsour

Hierarchical meso–macro structure porous carbon black as electrode materials in Li–air battery

Jun Kang [a,*], Oi Lun Li [c], Nagahiro Saito [a,b,c]

[a] Graduate School of Engineering, Nagoya University, Nagoya 464-8603, Japan
[b] Ecotopia Science Research Institute, Nagoya University, Nagoya 464-8603, Japan
[c] Green Mobility Collaborative Research Center, Nagoya University, Nagoya 464-8603, Japan

HIGHLIGHTS

- We report a new class of hierarchical structure porous carbon black.
- The carbon black has excellent meso–macro hierarchical pore structure.
- The hierarchical structure could enhance the cell performance of Li–air battery.
- This paper reported a novel synthesis method of meso–macro structure carbon black.

ARTICLE INFO

Article history:
Received 23 October 2013
Received in revised form
27 February 2014
Accepted 18 March 2014
Available online 26 March 2014

Keywords:
Solution plasma process
Porous carbon
Hierarchical meso–macro porous structure
Li–air battery

ABSTRACT

A new class of hierarchical structure porous carbon black, carbon nanoballs (CNBs), was generated by solution plasma process (SPP) with benzene. The structural characterization revealed that CNBs have excellent meso–macro hierarchical pore structure, with an averaged diameter size of 14.5 nm and a total pore volume of 1.13 $cm^3 g^{-1}$. The CNBs are aggregated forming inter-connected pore channels in different directions on both the meso- and macrometer length scales. The discharge capacity of CNBs reached 3600 mAh g^{-1}, which exceeded the capacity of Ketjen Black EC-600JD (a commercial carbon black with highest cell performance) by 30–40%. The excellent discharge capacity was contributed by the co-existence of high pore volume and meso–macro hierarchical porous structure. This new class carbon material exhibited higher discharge capacity compared to commercial porous carbon materials, and is possible to apply as the next generation of electrode materials in lithium–air (Li–air) battery. The structural and electrochemical properties accompanied with the synthesis mechanism of CNBs were discussed in details.

© 2014 Elsevier B.V. All rights reserved.

1. Introduction

Lithium–air (Li–air) battery, due to its high energy density, has a big potential for the application of future electrochemical power sources. It has a theoretical energy density equals to gasoline, and an energy density is 5–10 times greater than that of lithium-ion battery [1]. In the application of air electrode material in Li–air battery, porous carbon materials have an important role due to their remarkable porosity for oxygen diffusion.

Among various types of Li–air battery, non-aqueous system appears to be the safest accompanying with the highest rechargeability. During the discharge process, the non-soluble and non-conductive discharge by-product, Li oxides, are formed. In the porous air electrode, the pore entrances are easily blocked by these discharge products and thus the deeper reaction sites are still void yet inaccessible. Therefore, its actual discharge capacity often drops short compared to its theoretical value.

As the structure of carbon electrode has a great impact on the performance of Li–air battery, intensive efforts have been devoted to find out the important factors in designing a porous air electrode [2–5]. There are two key factors including pore size, pore volume which can affect the discharge capacity. Between them, larger pore volume allows more Li oxides to accommodate during discharge process. On the other hand, the entrance of the pores clogs easily if the pore size is too small, and hence the inner pore volume space cannot be accessed. Based on previous researches, a pore size <10 nm might be insufficient to sustain oxygen diffusion and might be blocked easily during cathode manufacturing despite using low

* Corresponding author. Tel./fax: +81 52 789 4699.
E-mail addresses: echemplasma@gmail.com, junkmu@naver.com (J. Kang).

http://dx.doi.org/10.1016/j.jpowsour.2014.03.072
0378-7753/© 2014 Elsevier B.V. All rights reserved.

amounts of binder [5–7]. Therefore, the pore size should be optimized to prevent clogging and enhance effective diffusion of oxygen over the entire pore network, while pore volume should be maximized to accommodate large amount of discharge by-products.

For this reason, recent studies has been focused on engineering carbon material consists of hierarchical pore structure (containing macropores and mesopores) [8,9]. The mesopores of this structure can serves for the storage of Li–O_2 products, and the macropores can function as "highways" to supply the oxygen into the inner regions of the air electrode during the discharge process. Therefore, it facilitates a continuous oxygen flow into air electrode without clogging.

In this article, a simple synthesis method of porous carbon nanoballs (CNBs) was being reported. CNBs were synthesized by solution plasma process (SPP) as described in our previous work [10]. Meanwhile, Ketjen Black EC-600JD (KB, Lion Corporation, Japan), a type of carbon blacks which has shown the highest discharge capacity among other commercial carbon materials, was compared to the results of CNBs. The difference of carbon structures were determined by the synthesis mechanism and process. In the structural characterization, it revealed that KB mainly consisted of micro–meso network while CNBs exhibited a hierarchical meso–macro pore structure. The effect of structural network on the discharge capacity and electrochemical properties were discussed in details. This paper not only reported a novel synthesis method of meso–macro structure carbon, but also suggested the hierarchical structure enhanced the cell performance of air electrode in Li–air battery.

2. Experimental procedures

2.1. Solution plasma processing

The plasma discharge was carried out at room temperature under atmospheric pressure conditions. A 100 (mL) glass vessel with a diameter of 5 cm and height of 7 cm was used as a reactor and pure benzene (99.5% Kanto chemical, Japan) was applied as the carbon precursor. A pair of tungsten electrodes (Φ1 mm, 99.95% Nilaco, Japan) was connected with a bipolar-DC pulse power supply (Kurita, Japan). Electrodes were insulated by ceramic tube and protruded length of 1.5 mm from ceramic tube tip to concentrate energy. The voltage, pulse frequency, pulse width, and electrode distance were controlled to be 1.6 kV, 15 kHz, 0.5 μs, and 1 mm, respectively. A schematic of experimental apparatus was being reported in other research paper by the author [10].

2.2. Drying of sample

After plasma discharge, the solution was filtered by glass microfiber filter (1.0 μm) and the residues (carbon) were dried at 70 °C for 1 h.

2.3. Heat treatment

Heat treatment was performed inside a tube furnace at 850 °C with a 20 min dwell time and under a flowing argon atmosphere. The heating rate and cooling rate were 25 and 7 °C min^{-1}, respectively.

2.4. Characterization of NPs/CNBs

2.4.1. Morphology of CNBs

Transmission electron microscope (TEM) observations were performed on JEM-2500SE at an acceleration voltage of 200 kV. Scanning electron microscope (SEM) images were obtained on JSM-6330F (JEOL) at an acceleration voltage of 5 kV.

2.4.2. Structural properties of CNBs and KB

The porous structure, cell performance and electrochemical properties of CNBs were compared to a type of commercial carbon black material, Ketjen Black EC-600JD (KB, Lion Corporation, Japan) in details. The BET surface area, total pore volume, and pore diameter were calculated from N_2 adsorption–desorption isotherms using the Brunauer–Emmett–Teller method which carried out on Belsorp-mini II. All samples were degassed at 200 °C for 2 h prior to the measurement of BET.

2.4.3. Electrical resistivity

The four-point probe method was applied to conduct the electrical resistivity test. Specimens were prepared by mixing 60 wt% of each carbon material with 40 wt% of polymer binder (PVDF, polyvinylidene fluoride, average Mw 534,000, Aldrich, Japan) by mortar and pestle for 10 min. After mixing, the powders were placed into a round die of inner diameter 10 mm, and compressed with a force of 8 Mpa of pressure at 25 °C for 5 min. The powder was compacted to pellets of 2 mm in thickness and 10 mm in diameter, and conducted to resistivity experiments.

2.4.4. Preparation of Li–air battery

To fabricate the air cathode, 0.2 g of carbon material were added into the mixture of 0.12 g of polyvinylidene fluoride (PVDF, average Mw 534,000, Aldrich, Japan) and 10 g of *N*-methyl pyrrolydone (NMP, Rikaken, Japan). The circular disks were obtained from the sheets of high-porosity copper foam (1.4 mm thickness, 600 μm average pore size) and submerged into the NMP/PVDF/carbon slurry. The copper disc was sonicated for 20 min in order to enhance the slurry penetration into the copper foam structure. To remove NMP, the cathodes were heated in dryer at 110 °C for 12 h. After drying, approximately 1.5 mg of carbon was loaded on the copper foam. The electrolyte was 1 M of $LiClO_4$ in an ethylene carbonate/propylene carbonate (EC/PC = 1:1) solution.

It should be noted that why EC/PC solvent has been chosen as electrolyte. Although ether- or glyme-based electrolytes are more stable than carbonate-based electrolytes during discharge, it has been reported that they also produce by-products such as Li carbonate and LiOH, instead of the desired Li_2O_2 [11–15]. Furthermore, they have a low contact angle on carbon with low O_2 solubility and hence tri-phase reaction sites will be reduced [16]. Meanwhile, cyclic carbonate-based electrolytes have a high polarity and their low affinity to carbon pores creates tri-phase reaction sites for electrochemical reaction [16]. By comparing different characteristics of electrolytes, EC/PC solvent was chosen in this experiment because we would like to solely evaluate the effect of cathode material's architecture on the electrochemical reaction (not rechargeability).

Lithium metal and glass microfiber filter (1.0 μm, Whatman, Japan) were used as the anode and separator, respectively. Type 2032 coin cell kits (Miclab, Japan) were used to fabricate cell devices and the cap of coin cells were drilled with 20 ∅1 mm pinholes to allow oxygen diffusion into the electrode. The Li–air cell was assembled in an argon-filled glove box. Before discharging, the air-cathode was soaked in electrolyte for 5 min in order to induce a good permeation of the electrolyte into the carbon materials. Cells were discharged in testing box which has a gas inlet and outlet. To avoid the negative effect of CO_2 and moisture, dry air (nitrogen 79%, oxygen 21%, humidity < 1%) flow through the box. The humidity inside testing box was less than 1% relative humidity measured by a BK Precision handheld humidity/temperature meter. The operation temperature and pressure were 25 °C and 1atm, respectively.

3. A hypothesis of synthesis mechanism and structure network in CNBs and KB

The hypothesis for the mechanism of CNBs by SPP is illustrated in Fig. 1. The porous properties were governed by the carbon particle aggregates. These aggregates can be understood by using the diffusion limited aggregation (D.L.A) model [17]. When carbon particles were generated in large amount directly from solution plasma, and these particles simultaneously undergone a random walk due to Brownian motion and these particles were combined together in different directions by collisions of individual particles. Carbon black (e.g. KB) in general, is generated from conventional plasma or combustion method has plentiful sprig, since a large number of particles were formed at once and the duration plasma (combustion) zone was relatively long. Thus, the particles were more likely to aggregate together and resulted in higher structure as shown in Fig. 1. In the case of SPP, the plasma zone was very small and the aggregates were quickly disturbed by the solution flux. In addition, the void volume between the particles of the aggregates (intra aggregate voids) and between aggregates was filled with liquid as soon as aggregates exited the plasma zone. Therefore, the structures of aggregates became simple as low structure because there was not enough time to grow. Thus, the majority of pore structure in CNBs and KBs was significantly different.

4. Results and discussions

4.1. Morphology of CNBs

On average, 500 mg of CNBs were generated from 100 ml of benzene with 20 min of SPP process. The morphology of the CNBs was observed under SEM and TEM, as shown in Fig. 2. These images revealed that the diameters of CNBs were ranged from 20 to 30 nm and these carbon spheres appeared as chain-like morphology with relatively regular size distribution. These particles aggregated forming inter-connected pore channels in different directions on both the meso- and macrometer length scales. In other words, the primary carbon particles arrange into agglomerates. Within these agglomerates, mesopores of 2–50 nm diameter exist. Agglomerates coalesce into chainlike aggregates, and a continuous network of pores is formed in the interstices thus mesopores were well connected with the macropores in all directions. Therefore, mesopores ascribed to the void space inside agglomerates, and meso- to macroporous space inside aggregates of agglomerates. The HRTEM image shows that CNBs is composed of continuous short graphene layers, and found to be parallel to the concentric direction with turbostratic structure.

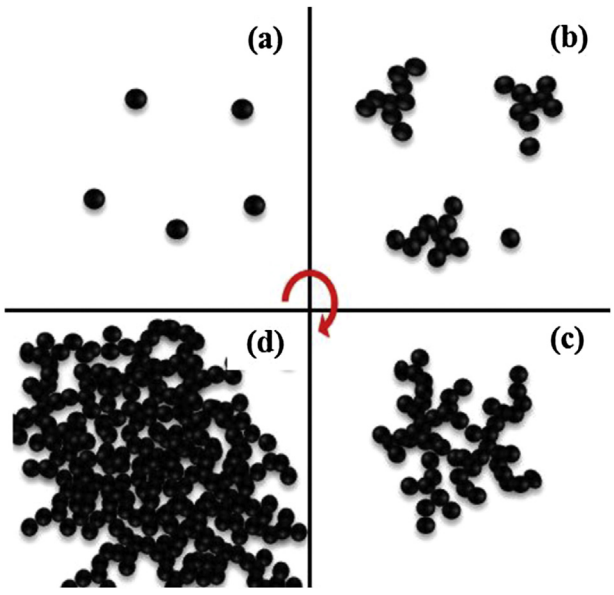

Fig. 1. Structure growth of carbon black: (a) carbonization → (b) aggregate → (c) low structure (meso–macropore) → (d) high structure (micro–mesopore).

4.2. Comparison of pore structure in CNBs and KB

The pore structure of CNBs and KB were investigated by N_2 adsorption–desorption method. Fig. 3a shows the isotherms of CNBs and KB it exhibited type IV characteristics according to the IUPAC classification and also demonstrated that the adsorption process of CNBs and KB consisted of three stages [18].

The steep initial region where $P/P_0 = 0–0.03$ indicated the filling of the micropores; compared to KB, the proportion of micropores in CNBs was very low. In second stage where $P/P_0 = 0.03–0.86$, CNBs illustrated a gradual slope of plateau, representing multilayer adsorption on the external surface. Meanwhile KB showed higher amount of multilayer compared to CNBs due to its high surface area. At higher relative pressures where $P/P_0 = 0.86–0.98$, a sharp slope was observed in the isotherm of CNBs and KB with a narrow hysteresis loop. This hysteresis is typically associated with capillary condensation which predicts the formation of mesoporous structures. Especially, the condensation occurs at higher relative pressure indicates the existence of larger pore size distribution. These results illustrated that CNBs possessed mainly mesopores with a large pore volume to accommodate N_2 molecular while KB consisted of hierarchical structure containing large portion of micropores.

Table 1 presents the detailed structural parameters including the Brunauer–Emmett–Teller (BET) theory surface area, total pore volume, and mean pore diameter of KB and CNBs. The BET surface area and total pore volume of CNBs were 314 $m^2\ g^{-1}$ and 1.13 $cm^3\ g^{-1}$, respectively. The resistivity value of CNBs was comparable to that of KB. The surface area and total pore volume of KB were a few times higher than that of the annealed CNBs; however, the mean pore diameter was majorly lower than 10 nm. According to the integral curves of the pore size distribution shown in Fig. 3b, the pore volume in the 2–10 nm diameter range of CNB was not observed, whereas in the large pore region, i.e., pores >10 nm, a drastic increase in the pore volume is observed. Therefore, it can be assumed that CNB has large pore volume in meso–macro range. On the contrary, KB has large pore volume in the region smaller than 50 nm. These characteristics clearly indicated that CNBs consisted of meso–macropore hierarchical structure while KB consisted of micro–mesopore hierarchical structure framework.

4.3. Discharge capacity

The voltage-capacity discharge experiments were carried out to evaluate the electrochemical performance of CNBs and KB. The performance of Li–air batteries are dependent on several factors, including carbon source, carbon loading, and electrolyte selection and volume [19–21]. For this reason, the experiments were carried out under same conditions mentioned in experimental procedures excluding carbon source. The discharge profile in Fig. 4 showed that the discharge capacity in CNBs reached 3600 mAh g^{-1} at 0.1 mA. The capacity of CNBs, disregarded of the discharge conditions, was approximately 30–40% higher than that of KB. The results implied a higher pore volume and surface area in KB, as observed in Table 1, did not necessary lead to a higher capacity. This phenomenon agreed with the suggestions of pore blockage of Li oxides by-

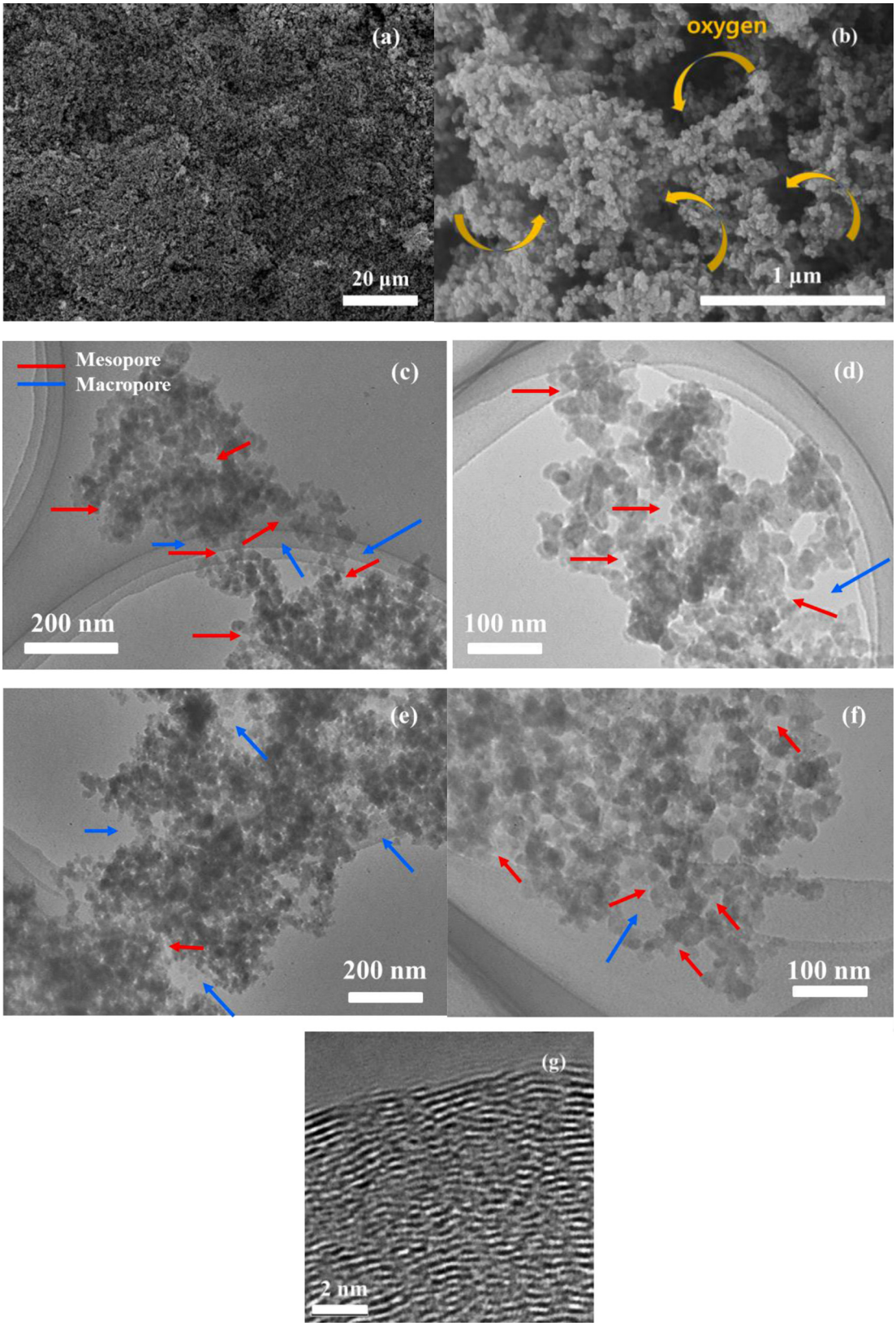

Fig. 2. (a–b) FESEM (c–f) TEM and (g) HRTEM image of CNBs, representative meso-, and macropores are indicated by arrows.

products and the micro–mesopore framework of KB limited the access of inner pore surface. Hence, the discharge capacities of meso–macropore based CNBs were superior to KB as the effective hierarchical structure was larger.

4.4. Electrochemical property

Fig. 5 shows the chrono-amperometric curves of air electrodes with discharge/charge potential. The curves evaluated the mass

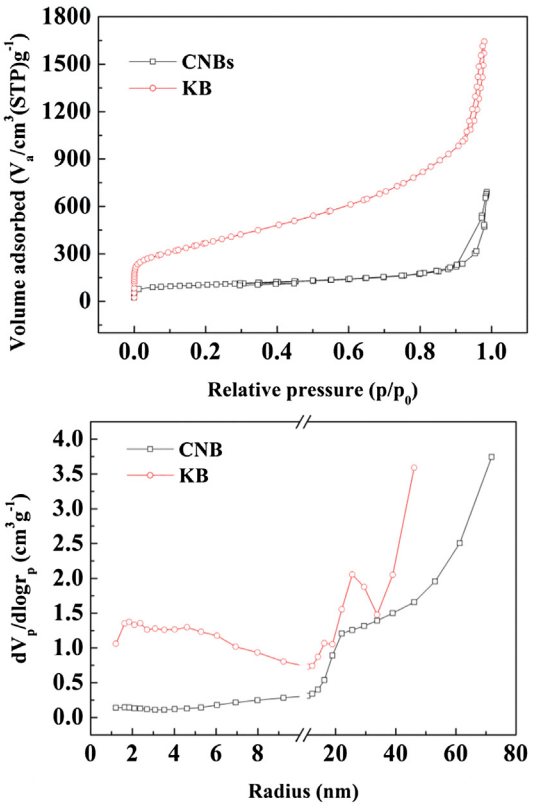

Fig. 3. Nitrogen adsorption–desorption isotherms of the CNBs (up) pore size distribution curves (down).

transport property of the materials inside the pores [22,23]. The cell voltage was stepped down from open circuit voltage (OCV) to below 0.6 V because the average discharge voltage of Li–air battery is usually around 2.5–2.6 V. This curves showed that the discharge current of CNBs was larger than that of KB at the same potential step. The results indicated that the hierarchical structure of CNBs maintained a higher electrochemical reaction and oxygen diffusion rate. These characteristics might be attributed to the effect of pore size. As the size of pore entrance is narrow, a mean collisional frequency between materials and carbon in the pathway increases. Thus diffusion resistance also increased and as a result, the mass transport rate to the inner pore decreased. Similar diffusion behavior was observed in Cottrell plot in Fig. 5(inset). The relationship between diffusion limiting current and diffusion coefficient can be described by the Cottrell Equation (1): [24]

$$I = nFAC_0\sqrt{\frac{D}{\pi t}} \quad (1)$$

where n is the number of electrons transferred in one electrochemical reaction step, F is the Faraday constant, A is the electrode area, D is the diffusion coefficient of oxygen in electrolyte, C_0 is the initial bulk concentration of oxygen in electrolyte and t is the time. The plot of I vs. $t^{-1/2}$ is linear and the diffusion coefficients D, can be

Table 1
Structural parameters/resistivity of annealed CNBs and KB.

Material	Surface area ($m^2\ g^{-1}$)	Pore volume ($cm^3\ g^{-1}$)	Mean pore diameter (nm)	Resistivity ($\Omega\ m^{-1}$)
CNBs	314.0	1.1	14.3	1.6
KB	1251.3	2.5	6.5	2.1

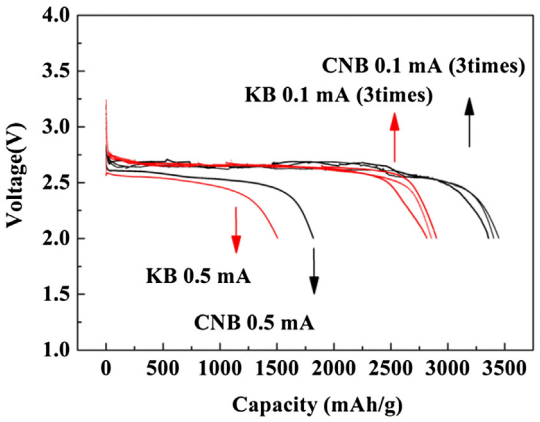

Fig. 4. Discharge curves of the Li–air cell.

obtained from the slope. From Fig. 5 (inset), the diffusion coefficient of CNBs was twice of that of KB. It implied that CNBs has a large diffusion pathway for higher mass transportation rate. The large pore entrance of CNBs might sustain a clear diffusion pathway during charging and discharging process because large pathway enabled high transport rates for both Li ions and oxygen to the reaction sites deep inside the pore.

Fig. 6 shows the impedance spectra of the discharged CNBs and KB at rate of 0.1 mA cm^{-2} under dry air environment before and after discharge. A depressed semicircle was observed in high frequency region while a straight line appeared at low frequency. The equivalent-circuit parameters were obtained by curve fitting using the Z view software (Solartron) with the equivalent circuit shown in Fig. 6. The model impedance spectrum curve showed a good match with the experimental impedance spectrum over the entire frequency range. The circuit elements can be defined as follows: R_b is bulk resistance of the cell, which includes contributions from electric conductivity of the electrolyte, separator, and electrodes [25,26]. R_{ct} and CPE are corresponded to interface resistance relates to the combination of the faradic charge-transfer resistance [25,27]. The linear Warburg element following the semicircle was attributed to the kinetic resistance related materials (Li ions) diffusion [28]. The impedance spectra showed that the R_b of both CNBs and KB were very similar, indicating that the electrodes have equal combined resistance of the carbon materials, ionic resistance of the electrolyte, and contact resistance between the material and the current collector. On the other hand, charge transfer resistance of CNBs increased more significantly compared to that of KB after discharging process. During discharge, the non-conductivity Li oxide by-products deposited on the surface of carbon and reduced

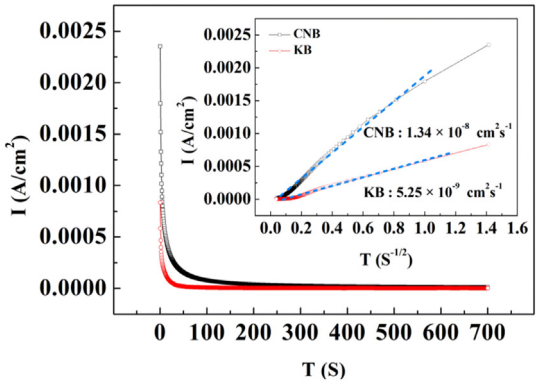

Fig. 5. Chronoamperometry curve, Cottrell plot (inset).

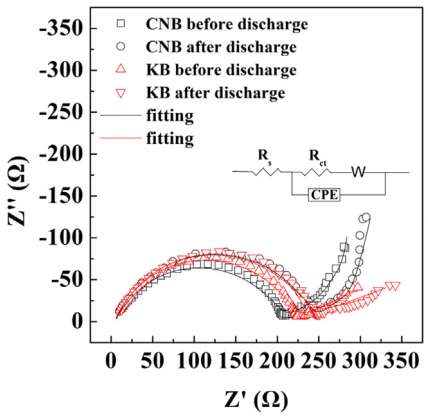

Fig. 6. Impedance spectra of the Li–air cell.

the electronic conductivity of the cathode, which also led to the increase of the interfacial resistance between electrode and electrolyte. Therefore, if the amount of Li oxide deposited on surface of carbon increased, R_{ct} increased accordingly. This result also agreed with the result of the discharge capacity in Fig. 4.

Meanwhile, the equivalent-circuit parameter showed that the pure capacitors component was replaced by CPE, which associated with the degree of non-ideality and resulted in depressing spectra [29–34]. High content (40 wt%) of binder (PVDF) in electrode might disturb the ion mobility or adsorption on active site over the entire frequency range and thus might affect the ideal capacitive behavior. Generally, double layer which exists at the interface between an electrode and its surrounding electrolyte does not often behave exactly as an ideal capacitor, due to the fact that charges on the electrolyte side of the capacitor are distributed in diffuse layer by distribution of active sites on the combination of carbon and PVDF surface.

The impedance spectra at low frequency showed that the imaginary part of the impedance of CNBs was larger than that of KB at same frequency. The behavior might be explained by the difference of pore diameter in carbon materials. With decreasing frequency, the electrolyte ions began to penetrate deeper into the porous, then larger electrode surface area became available for ion adsorption, resulting in an increment in imaginary part of the impedance. However, in the case of KB, it has large portion of micropores and hence the diffusion of Li ion can be interrupted by small orifices, thus led to a lower contribution to imaginary part at same frequency.

In terms of electrochemical performance, the micro–mesopore structure in KB might be easily clogged and restrict the accessibility of the inner pores. In contradiction, the meso–macropore in CNBs ensured higher diffusion rate for Li oxide accommodation and avoided pore blockage. As a result, the effective pore structure for the Li–air reaction in CNBs was larger and exhibited a higher discharge capacity compared to KB.

5. Conclusions

500 mg of spherical carbon nano particles, named carbon nanoballs (CNBs), were synthesized successfully by the solution plasma process (SPP) from 100 ml benzene solution within 20 min. In the hypothesis of the synthesis process, it was assumed that the plasma zone was very small and the aggregations built by the reaction zone were quickly circulated by solution flux. Therefore, the structures of aggregations became simple (low structure) because the growth time was limited. The structure characteristics proved that the synthesized CNBs have excellent meso–macro hierarchical pore structure, with an averaged diameter size of 14.5 nm and a total pore volume of 1.13 $cm^3\ g^{-1}$. The electrical capacity performance of CNBs reached 3600 mAh g^{-1}, which was approximately 30–40% higher than that of Ketjen Black EC-600JD, a commercial carbon material which demonstrated the highest capacity. It was proposed that the meso–macro hierarchical pore structure with high pore volume was more effective and encouraged higher electrochemical reaction and oxygen diffusion. These factors, as a result, could contribute to a high discharge capacity in CNBs. SPP synthesis method can provide unique mesopore structure in CNBs and this type of new class carbon, with its high discharge capacity, might bring the application of Li–air battery one step forward.

References

[1] I. Kowalczk, J. Read, M. Salomon, Pure Appl. Chem. 79 (2007) 851–860.
[2] J. Xiao, D.H. Wang, W. Xu, D.Y. Wang, R.E. Williford, J. Liu, J.G. Zhang, J. Electrochem. Soc. 157 (2010) A487–A492.
[3] T. Kuboki, T. Okuyama, T. Ohsaki, N. Takami, J. Power Sources 146 (2005) 766–769.
[4] M. Mirzaeian, P.J. Hall, J. Power Sources 195 (2010) 6817–6824.
[5] X.H. Yang, P. He, Y.Y. Xia, Electrochem. Commun. 11 (2009) 1127–1130.
[6] C. Trana, X.Q. Yang, D. Qua, J. Power Sources 195 (2010) 2057–2063.
[7] R. Younesia, N. Singha, S. Urbonaitea, K. Edströma, ECS Trans. 25 (2010) 121–127.
[8] R.E. Williford, J.G. Zhang, J. Power Sources 194 (2009) 1164–1170.
[9] J. Xiao, D.H. Mei, X.L. Li, W. Xu, D.Y. Wang, G.L. Graff, W.D. Bennett, Z.M. Nie, L.V. Saraf, I.A. Aksay, J. Liu, J.G. Zhang, Nano Lett. 11 (2011) 5071–5078.
[10] J. Kang, O.L. Li, N. Saito, Carbon 60 (2013) 292–298.
[11] B.D. McCloskey, D.S. Bethune, R.M. Shelby, G. Girishkumar, C. Luntz, J. Phys. Chem. Lett. 2 (2011) 1161–1166.
[12] C.O. Laoire, S. Mukerjee, K. Abraham, E. Plichta, M. Hendrickson, J. Phys. Chem. C 114 (2010) 9178–9186.
[13] C.O. Laoire, S. Mukerjee, E.J. Plichta, M.A. Hendrickson, K.M. Abraham, J. Electrochem. Soc. 158 (2011) A302–A308.
[14] S.A. Freunberger, Y.H. Chen, N.E. Drewett, L.J. Hardwick, F. Barde, P.G. Bruce, Angew. Chem. Int. Ed. 37 (2011) 8609–8613.
[15] D. Xu, Z.L. Wang, J.J. Xu, L.L. Zhang, X.B. Zhang, Chem. Commun. 48 (2012) 6948–6950.
[16] J. Read, Electrochem. Soc. 10 (2009) A773–A779.
[17] T.A. Witten, L.M. Sander, Phys. Rev. Lett. 19 (1981) 1400–1403.
[18] J. Rouquerol, D. Avnir, C.W. Fairbridge, D.H. Everett, J.M. Haynes, N. Pernicone, J.D.F. Ramsay, K.S.W. Sing, K.K. Unger, Pure Appl. Chem. 8 (1994) 1739–1758.
[19] S.S. Zhang, D. Foster, J. Read, J. Power Sources 195 (2010) 1235–1240.
[20] S.D. Beattie, D.M. Manolescu, S.L. Blair, J. Electrochem. Soc. 156 (2009) A44–A47.
[21] C.K. Park, S.B. Park, S.Y. Lee, H. Lee, H. Jang, W.I. Cho, Bull. Korean Chem. Soc. 31 (2010) 3221–3224.
[22] D. Gerteisen, T. Heilmann, C. Ziegler, J. Power Sources 177 (2008) 348–354.
[23] H. Weydahl, S. Møller-Holst, G. Hagen, B. Børresen, J. Power Sources 171 (2007) 321–330.
[24] A.J. Bard, L.R. Faulkner, Electrochemical Methods Fundamentals and Applications, Wiley, New York, 2001.
[25] J.Y. Song, H.H. Lee, Y.Y. Wang, C.C. Wan, J. Power Sources 111 (2002) 255–267.
[26] H. Wang, H. Huang, S.L. Wunderz, J. Electrochem. Soc. 147 (2000) 2853–2861.
[27] X. Yang, Y. Xia, Solid State Electrochem. 14 (2010) 109–114.
[28] F. Croce, F. Nobili, A. Deptula, W. Lada, R. Tossici, A. D'Epifanio, B. Scrosati, R. Marassi, Electrochem. Commun. 12 (1999) 605–608.
[29] J.R. Macdonald (Ed.), Impedance Spectroscopy, John Wiley & Sons, New York, 1987.
[30] W.H. Mulder, J.H. Sluyters, T. Pajkossy, I. Nyikos, J. Electroanal. Chem. 285 (1990) 103–115.
[31] C.H. Kim, S.I. Pyun, J.H. Kim, Electrochim. Acta 48 (2003) 3455–3463.
[32] C.A. Schiller, W. Strunz, Electrochim. Acta 46 (2001) 3619–3625.
[33] J.B. Jorcin, M.E. Orazem, N. Pebere, B. Tribollet, Electrochim. Acta 51 (2006) 1473–1479.
[34] K.B. Oldham, Electrochem. Commun. 6 (2004) 210–214.